RSC Advances

PAPER

View Article Online
View Journal | View Issue

Cite this: *RSC Adv.*, 2021, **11**, 36689

Investigation on the upconversion luminescence and ratiometric thermal sensing of $SrWO_4:Yb^{3+}/RE^{3+}$ (RE = Ho/Er) phosphors

Hang Liu, Xiukai Jian, Mingtai Liu, Kailin Wang, Guangyao Bai and Yuhong Zhang *

Received 8th September 2021
Accepted 8th November 2021

DOI: 10.1039/d1ra06745a

rsc.li/rsc-advances

$SrWO_4$ phosphors doped with $Ho^{3+}(Er^{3+})/Yb^{3+}$ are successfully prepared by a high temperature solid-state reaction method. The upconversion (UC) luminescence properties of all the samples have been investigated under 980 nm excitation. Strong green emissions are obtained in the $SrWO_4:Yb^{3+}/Ho^{3+}$ and $SrWO_4:Yb^{3+}/Er^{3+}$ samples with the naked eyes. In a temperature range going from 303 K to 573 K, the UC emission spectra of the phosphors have been measured. Then the temperature sensing properties also have been discussed *via* fluorescence intensity ratio (FIR) technology. For the $SrWO_4:Yb^{3+}/Ho^{3+}$ phosphor, the FIR technologies based on thermal coupling levels (TCLs)($^5F_4$,$^5F_5$) and non-thermal coupling levels (non-TCLs)($^5S_2$, $^5F_4/^5F_5$) are used for investigating the sensitivity. The results show that the maximum absolute sensitivity reaches 0.0158 K^{-1} with non-TCLs. As for Yb^{3+}/Er^{3+} codoped $SrWO_4$ phosphor, the maximum absolute sensitivity reaches 0.013 K^{-1} with TCLs ($^2H_{11/2}$,$^4S_{5/2}$) at a temperature of 513 K. These significant results demonstrate that the $SrWO_4:Ho^{3+}(Er^{3+})/Yb^{3+}$ phosphors are robust for optical temperature sensors.

1. Introduction

As the basic parameter of thermodynamics, temperature measurement plays a vital role in scientific research, industrial production and medicine.[1] In recent years, much attention has been paid to non-contact temperature sensors based on rare earth (RE) ion activated luminescent materials.[2] Some UC luminescent materials with doping of RE^{3+} ions have been studied for temperature sensors.[3–7] The FIR technology based on the measurement of the temperature-dependent FIR from two excited state energy levels of activators represents an accurate temperature measuring method, because the FIR from the thermally coupled levels (TCLs) of RE ions is independent of the excitation intensity fluctuations, external disturbance and spectrum losses. Thus, reasonable measurement accuracy and sensitivity could be obtained with this method. The variation of FIR is generally caused by a thermally induced population re-distribution among the TCLs. And some RE ions have already been explored for designing FIR thermometry, such as Er^{3+}, Tm^{3+}, Ho^{3+} *et al.*[8–13] The sensitivity is an important role of a temperature sensing device. The absolute sensitivity is defined as the rate of change of FIR with change in temperature relative to FIR. Basically, a larger energy gap between the TCLs benefits the enhancement of sensitivity. However, the largest energy mismatches between those TCLs cannot exceed 2000 cm^{-1}, so it is difficult for the further improvement of sensitivity. There is an urgent need to design a new temperature measurement method to obtain high detecting sensitivity. Recently, a new kind of strategy has been proposed to solve the above drawback, which is based on FIR between the non-TCLs of the activators. The FIR derived from non-TCLs is also related to temperature. Compared with the FIR technique based on the TCLs, the FIR technique based on the non-TCLs is no longer limited by the energy gap. The Er^{3+} and Ho^{3+} ions also have non-TCLs pairs in addition to TCLs. So further investigation on temperature sensing properties of Er^{3+} and Ho^{3+} ions based on the FIR technology (TCLs and non-TCLs) is necessary.

Besides activators, temperature sensing properties of UC luminescent materials are also decided by host material. Among various hosts, tungstates have obtained much attention because of their brilliant physical and chemical stability, low phonon threshold energy, and high density.[14] The Ln^{3+} ions also have high doped concentration in tungstates host. So the activators can emit intense and stable fluoresce even at high temperature.[15] $SrWO_4$ belongs to a body-centered tetragonal system with scheelite crystal structure where WO_4^{2-} molecular ions are loosely bound to Sr^{2+} cations. It has been reported that $SrWO_4$ is an ideal host for optical temperature sensing materials. Recently, the temperature sensing properties of Ln^{3+} doped tungstates also have been studied. Pandey *et al.* report that the Er^{3+}–Yb^{3+} co-doped $SrWO_4$ phosphor is a good optical temperature sensing material, and its maximum absolute sensitivity reaches 0.01498 K^{-1}.[16] The high sensitivity of Tm^{3+}/Yb^{3+} co-doped $SrWO_4$ phosphor for optical thermometry is synthesized by Song *et al.*, and when the temperature is 323 K, the absolute sensitivity reaches a maximum of 0.00617 K^{-1}.[17] For Sm^{3+} doped $SrWO_4$ phosphor and Nd^{3+}/Yb^{3+} co-doped

School of Electrical and Computer Engineering, Jilin Jianzhu University, Changchun 130118, China. E-mail: zhangyuhong@jlju.edu.cn; Liuhang76@163.com

$SrWO_4$ phosphor, they also have good temperature sensing performance.[18,19] Note that, the $SrWO_4$ material is more suitable to be a UC fluorescence host for designing optical temperature sensor. However, as far as we know, the $SrWO_4$:Yb^{3+}/Ho^{3+} phosphor for optical thermometry has not been investigated. There are even fewer reports on its optical thermometry using FIR technique based on the non-TCLs.

In this paper, the $SrWO_4$:Yb^{3+}/RE^{3+}(RE = Er, Ho) phosphors are synthesized by a high temperature solid state reaction. The UC luminescence performances and temperature sensing properties are investigated under 980 nm excitation. The experimental results illustrate that the temperature sensitivity of our phosphors are better than the most reported Ho^{3+}(Er^{3+}) doped materials. The $SrWO_4$ doping Ho^{3+}(Er^{3+}) ions materials are optical temperature sensing material with good application value.

2. Experimental

2.1 Synthesis of the phosphor

The samples are designed according to the molar composition of $Sr_{1-x-0.01}Yb_xHo_{0.01}WO_4$ (x = 0, 1%, 2%, 3%, 4%, 6%, 10%) and $Sr_{1-y-0.01}Yb_yEr_{0.01}WO_4$ (y = 0, 1%, 2%, 3%, 4%), and synthesized by solid-state reaction method. High-purity $SrCO_3$ (99%), WO_3 (99.8%), Yb_2O_3 (99.99%), Ho_2O_3 (99.99%) and Er_2O_3 (99.99%) are purchased from Aladdin Chemical Reagent Co. Ltd (China). The raw materials are weighed by molar ratio and mixed together. The mixtures thoroughly are ground in a mortar of agate for 60 minutes. The ground mixture is transferred to a crucible ceramics and then heated it in a muffle furnace. First, the temperature rises to 900 °C by 10 °C min^{-1}. The samples are kept at 900 °C for 4 h. Next, temperature is increased by 5 °C min^{-1} to 1100 °C and kept for 6 h. Finally the $SrWO_4$:Ho^{3+}/Yb^{3+} and $SrWO_4$:Er^{3+}/Yb^{3+} phosphors are obtained.

2.2 Measurement and characterization

The structural formation of the phosphors has been measured using an X-ray diffraction (Rigaku D/Max-2500) in the range of 15° to 80° (2θ), and its radiation source is Cu Kα ray of λ = 0.15406 nm. For morphology and size of the phosphors, the field emission scanning electron microscope (FE-SEM, JEOL JEM-6700F) is used to perform. The UC emission spectra are recorded using the Zolix Omni-λ500 spectrometer under a 980 nm laser (MDL-III-980-2W, China) excitation. The samples are heated using an Orient KOJI TAP-02 high temperature thermometer, among a temperature range of 303 to 573 K, with a temperature control accuracy of 0.1 °C.

3. Result and discussion

3.1 Structural characterization

Fig. 1(a) shows the XRD patterns of the $SrWO_4$:Ho^{3+}/Yb^{3+} phosphors. It can be seen that the diffraction peaks of the samples are very consistent with the standard card of $SrWO_4$ (JCPDS no. 08-0490). The sharp and strong diffraction peaks show that the synthesized samples are crystallized well. It also means that Sr^{2+} in the $SrWO_4$ lattice is substituted by Ho^{3+} and Yb^{3+} ions. The XRD patterns of the $SrWO_4$:Er^{3+}/Yb^{3+} samples are shown in Fig. 1(b). The main diffraction peaks of samples are also consistent with the standard card of $SrWO_4$ (JCPDS no. 08-0490). But an extra weak peak at 29.3° appears in $SrWO_4$:1% Er^{3+}, x%Yb^{3+}(x = 2, 3, 4) samples, which may be induced by the minor unreacted component of Yb_2O_3. Once the concentration of the Yb^{3+} ions is over 2%, a part of the Yb^{3+} ions will not be added in the lattice. In addition, the peak at 30°moves to a high angle direction with the concentration of Yb^{3+} ions increasing (see the illustration in Fig. 1(b)), which is attributed to the shrinkage of the crystal lattice caused by the doped Er^{3+} and Yb^{3+} ions substituting the Sr^{2+} sites. The ionic radius of Er^{3+}, Yb^{3+} and Sr^{2+}(Er^{3+}: 0.89 Å, Yb^{3+}: 0.86 Å and Sr^{2+}: 1.12 Å)are different, so the crystal lattice will produce deformation. The SEM images of $SrWO_4$:Ho^{3+}(Er^{3+})/Yb^{3+} phosphor are shown in Fig. 2. It indicates that the size of the prepared phosphor is almost uniform.

3.2 Upconversion emission properties

Fig. 3(a) shows the UC emission spectrum of $SrWO_4$:1%Ho^{3+}/ 2%Yb^{3+} phosphor from 500 to 800 nm under 980 nm excitation. Three characteristic emission bands are presented that the strong green emission (~540 nm) belongs to the radiative

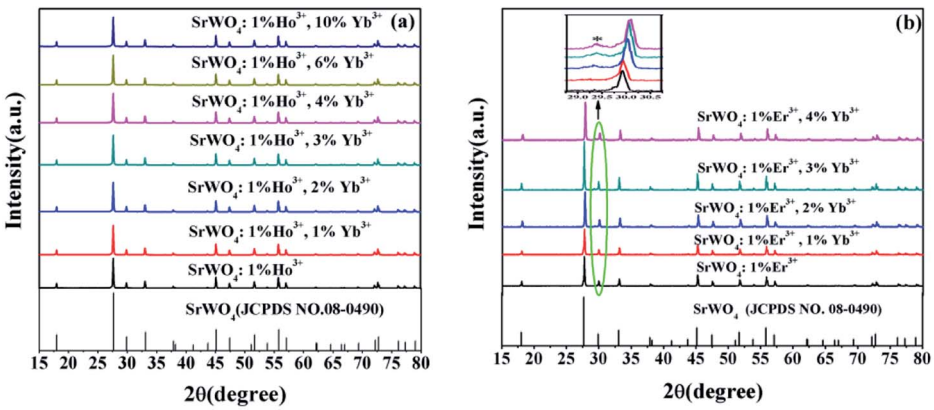

Fig. 1 XRD patterns of $SrWO_4$: (a) 1%Ho^{3+}/x%Yb^{3+}(x = 0, 1, 2, 3, 4, 6, 10) phosphors. (b) 1%Er^{3+}/x%Yb^{3+}(x = 0, 1, 2, 3, 4) phosphors.

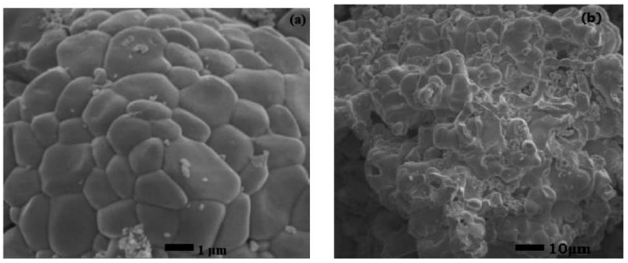

Fig. 2 SEM images of $SrWO_4$: (a) 1%Ho^{3+}/2%Yb^{3+} phosphor. (b) 1% Er^{3+}/1%Yb^{3+} phosphor.

transition from the $^5S_2/^5F_4$ to $^5I_8$, the red emission (~663 nm) belongs to the radiative transition from $^5F_5$ to $^5I_8$ and the weak near infrared emission (~756 nm) corresponds to $^5F_4 \rightarrow {}^5I_7$ energy level transition of Ho^{3+} ions. Fig. 3(b) shows the UC emission spectra of $SrWO_4$:1%Ho^{3+}/x%Yb^{3+} ($x = 0, 1, 2, 3, 4, 6, 10$). It is seen that, the intensities of all the UC emission peaks reach maximum values at $x = 2$. But they decrease if the Yb^{3+} concentration is further increased up to 2%. The Yb^{3+} ion is a high-efficiency sensitizer for Ho^{3+} ion because it has lager absorption cross-sectional area at the near infrared. With increasing the Yb^{3+} ions concentration to 2%, the energy transfer process from Yb^{3+} to Ho^{3+} can be enhanced, resulting in higher UC emission intensity. However, with the further enhancement of the Yb^{3+} concentrations, the distance between the doping ions decreases with the increase of Yb^{3+} concentration. It induces more intense interaction among adjacent Yb^{3+} ions, which cause concentration quenching.[20]

In order to explicate the possible UC emission process of the $SrWO_4$:Ho^{3+}/Yb^{3+} sample, the dependence relation of the UC emission intensity *via* pump power is measured. The relationship between UC emission intensity and pumping power can be described by the following eqn (1):[21]

$$I \propto P^n \quad (1)$$

where I is the UC emission intensity, P is the pumping power and n is the photon numbers which correspond to populate the upper emitting levels. Fig. 3(c) shows the log–log plot of intensity *versus* pump power and the slopes of the fitted lines of $SrWO_4$:1%Ho^{3+}/2%Yb^{3+} sample. It can be seen that n values are 1.21, 1.24 and 2.27 for green (~540 nm), red (~663 nm), and near-infrared (~756 nm) emissions. It indicates that these UC emission processes are related to the two-photon processes. The energy level diagrams of Ho^{3+}/Yb^{3+} ions and possible UC emission processes are shown in Fig. 3(d).

Under 980 nm excitation, the Yb^{3+} ion are excited from the ground state $^2F_{7/2}$ to the excited state $^2F_{5/2}$ by ground state absorption (GSA) process. Ho^{3+} ions are excited to the excited state levels mainly through the energy transfer (ET) process from Yb^{3+} to Ho^{3+}. Through ET1 ($^2F_{5/2}$ (Yb^{3+}) + $^5I_8$ (Ho^{3+}) → $^2F_{7/2}$ (Yb^{3+}) + $^5I_6$ (Ho^{3+})), the Ho^{3+} ions are excited from the $^5I_8$ to the $^5I_6$ state.[22] Some Ho^{3+} ions at $^5I_6$ state can nonradiatively (NR) relax to $^5I_7$ state, and then populating the $^5F_5$ state by excited state absorption (ESA) from $^5I_7$ to $^5F_5$. Ho^{3+} ions at $^5I_6$ state can continue to be excited into the $^5S_2$, $^5F_4$ coupling state by ET2 ($^2F_{5/2}$ (Yb^{3+}) + $^5I_6$ (Ho^{3+}) → $^2F_{7/2}$ (Yb^{3+}) + $^5S_2$, $^5F_4$ (Ho^{3+})). Subsequently, the Ho^{3+} ions at the $^5S_2$, $^5F_4$ coupling state will relax to the $^5F_5$ state by NR relaxation, and then a part of the Ho^{3+} ions at the $^5F_5$ state are transferred to the $^5I_8$ state, concurrently red light of 663 nm is emitted. The $^5S_2$, $^5F_4$ coupling state relax to the $^5I_8$ and $^5I_7$ states, resulting in high

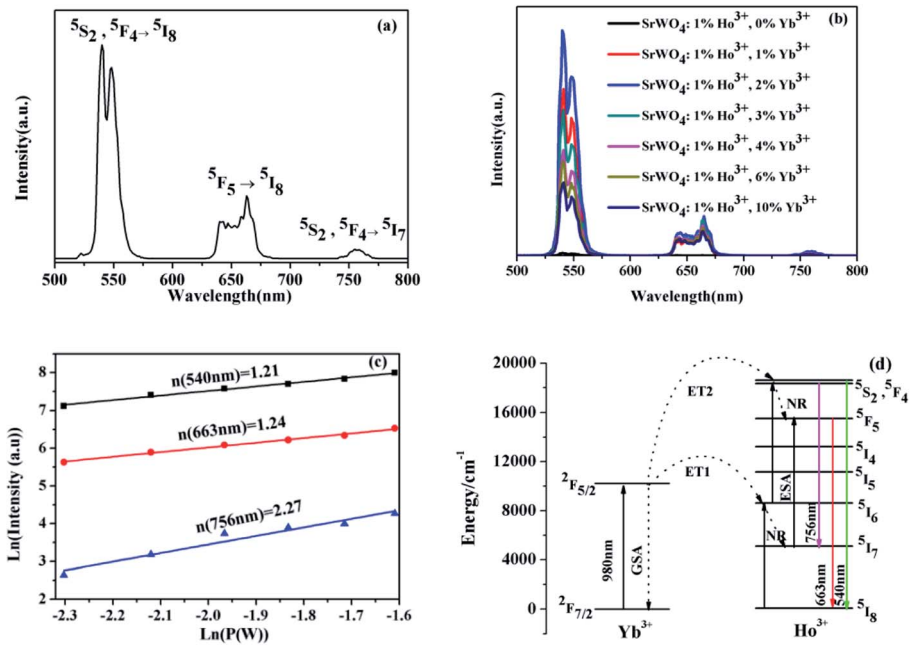

Fig. 3 (a). The emission spectrum of $SrWO_4$:1%Ho^{3+}/2%Yb^{3+} phosphor from 500 to 800 nm under exciting at 980 nm. (b). The UC emission spectra of $SrWO_4$:1%Ho^{3+}/x%Yb^{3+} ($x = 0, 1, 2, 3, 4, 6, 10$). (c). Log–log diagram of excitation power density and UC emission intensity. (d). The energy level diagrams of Ho^{3+}/Yb^{3+} ions and possible UC emission processes.

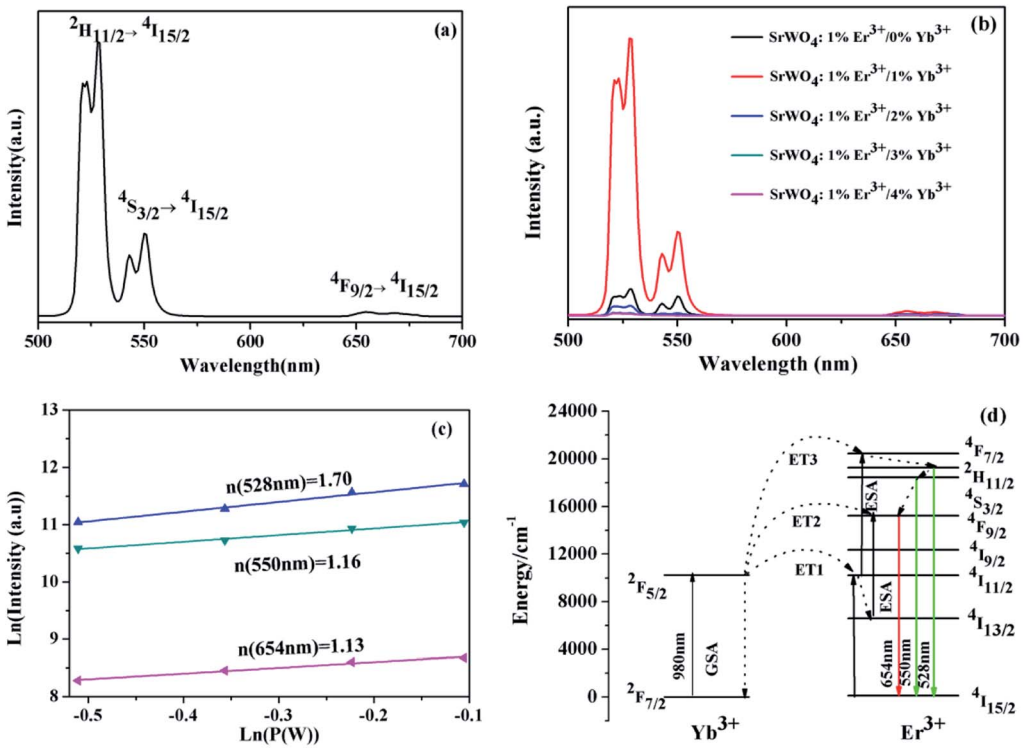

Fig. 4 (a). The UC emission spectrum of $SrWO_4$:1%Er^{3+}/1%Yb^{3+} phosphor. (b). UC emission spectra of $SrWO_4$:1%Er^{3+}/x%Yb^{3+} ($x = 0$, 1, 2, 3, 4). (c). Log–log relationship between pump power and UC emission intensity of $SrWO_4$:1%Er^{3+}/1%Yb^{3+} phosphor. (d). The energy level diagrams of Er^{3+}/Yb^{3+} ions and possible UC emission processes.

intensity green light (~540 nm) and low intensity red light (~756 nm), respectively.

The UC emission spectrum of $SrWO_4$:1%Er^{3+}/1%Yb^{3+} phosphor is shown in Fig. 4(a). Two UC emission bands are exhibited, the strong green and the weak red emission, which can be attributed to the radiative transitions from $^2H_{11/2}$/$^4S_{3/2}$ to $^4I_{15/2}$ and the $^4I_{9/2} \rightarrow {}^4I_{15/2}$ of the Er^{3+} ions, respectively. Fig. 4(b) shows the UC emission spectra of $SrWO_4$:1%Er^{3+}/x%Yb^{3+} ($x = 0$, 1, 2, 3, 4). It can be found that the intensities of two emission bands first increase and then decrease with increasing Yb^{3+} concentrations, and reach a maximum at $x = 1$. Once the concentration of Yb^{3+} is over 1%, the UC emission intensities rapidly decline. This is mainly attributed to that the energy transfer efficiency from Yb^{3+} to Er^{3+} ion decrease because the limit of the Yb^{3+} that can be stabilized into the matrix. As demonstrated by the extra peaks in the XRD patterns, when the concentration of the Yb^{3+} ions is over 2%, a part of the Yb^{3+} ions will not be added in the lattice.

The dependence relationship of the UC emission intensities of $SrWO_4$:Er^{3+}/Yb^{3+} on pump power are shown in Fig. 4(c). For the emission ~528 nm, 550 nm and 654 nm, the slopes of the fitting experiment data are 1.70, 1.16 and 1.13, which is near 2. It indicates that all emission processes are related to the two-photon processes. Fig. 4(d) shows the energy level diagrams and possible UC emission processes of Er^{3+} and Yb^{3+} ion. Under 980 nm laser excitation, Yb^{3+} ions are excited from the ground state $^2F_{7/2}$ to the excited state $^2F_{5/2}$ by GSA process. The Er^{3+} ions are excited to the $^4I_{11/2}$ state from the ground state through the ET1 ($^2F_{5/2}$ (Yb^{3+}) + $^4I_{15/2}$ (Er^{3+}) → $^2F_{7/2}$ (Yb^{3+}) + $^4I_{11/2}$ (Er^{3+})). After that, the Er^{3+} ions at $^4F_{7/2}$ state can be populated from the $^4I_{11/2}$ state by the ET3 ($^2F_{5/2}$ (Yb^{3+}) + $^4I_{11/2}$ (Er^{3+}) → $^2F_{7/2}$ (Yb^{3+}) + $^4F_{7/2}$ (Er^{3+})). The $^2H_{11/2}$ and $^4S_{3/2}$ states are populated from the $^4F_{7/2}$ state owing to the NR relaxation, and then the Er^{3+} ions at $^2H_{11/2}$ and $^4S_{3/2}$ states relax to the $^4I_{15/2}$ state, leading to the green UC emissions (528 nm and 550 nm). The Er^{3+} ions at $^4I_{11/2}$ state can relax to the $^4I_{13/2}$ state through the multiphonon relaxation (MPR) process, and then the Er^{3+} ions at $^4I_{13/2}$ state are excited to the $^4F_{9/2}$ by ET2 ($^2F_{5/2}$ (Yb^{3+}) + $^4I_{13/2}$ (Er^{3+}) → $^2F_{7/2}$ (Yb^{3+}) + $^4F_{9/2}$ (Er^{3+})). Meanwhile, the $^4F_{9/2}$ state can be also populated from the $^4S_{3/2}$ state through the NR relaxation. The Er^{3+} at the $^4F_{9/2}$ state will transit to the $^4I_{15/2}$ state and thus emitted the red light (~654 nm).

3.3 Optical temperature-sensing properties

For investigating the optical temperature sensing characteristics of $SrWO_4$:Ho^{3+}/Yb^{3+} phosphor, the emission spectra of the $SrWO_4$:Ho^{3+}/Yb^{3+} sample are measured at different temperature. As shown in Fig. 5(a), it can be seen that the UC emission intensities of all emission band decrease with the temperature increasing. The possible reason is thermal quenching effect.[23] But the decreasing rate of the different emission band is different. Fig. 5(b) shows the UC emission intensity variation of 540 nm ($^5S_2$, $^5F_4 \rightarrow {}^5I_8$) and 756 nm ($^5S_2$, $^5F_4 \rightarrow {}^5I_7$) with temperature increasing. It is clearly observed that the UC emission intensity at 756 nm drops much more slowly than that at 540 nm with the temperature increasing. By considering the

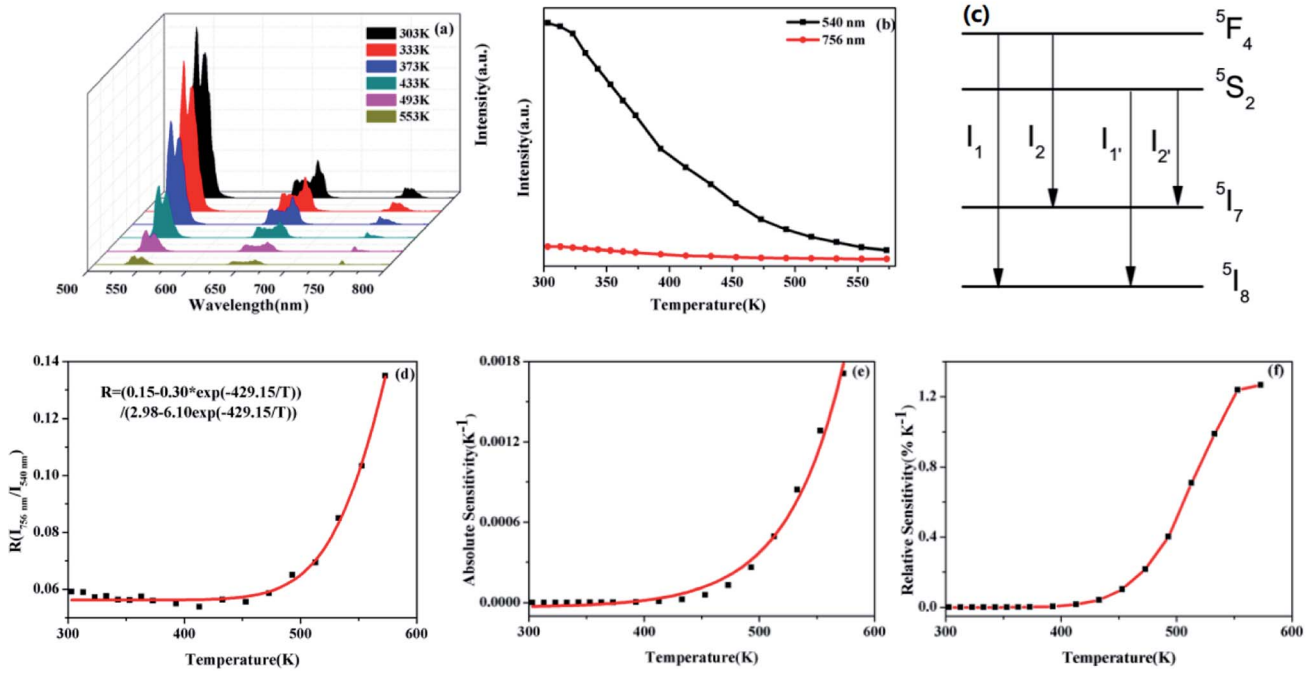

Fig. 5 (a). Temperature-dependent on UC emission spectra of $SrWO_4$:1%Ho^{3+}/2%Yb^{3+} phosphor at 303–573 K. (b). The emission intensity of $SrWO_4$:1%Ho^{3+}/2%Yb^{3+} phosphor center at 540 nm and 756 nm change in the range 303–573 K. (c) Four-level simplified diagram of transitions from adjacent excited levels to two lower levels. (d) The FIR ($I_{756\ nm}/I_{540\ nm}$), (e) the absolute sensitivity based on the $I_{756\ nm}/I_{540\ nm}$ (f) the relative sensitivity based on the $I_{756\ nm}/I_{540\ nm}$.

thermalization between $^5S_2$ and $^5F_4$ levels, the FIR of the UC emission from ($^5F_4$, $^5S_2$) → $^5I_8$ and ($^5F_4$, $^5S_2$) → $^5I_7$ transitions can be analyzed by using a four-level system, which was introduced by González-Pérez *et al.*[24] as shown in Fig. 5(c). The $^5S_2$, $^5F_4$, $^5I_7$ and $^5I_8$ levels form a four-level system. The emission intensity is proportional to the population of each energy level and the population of the excited state relates to the temperature. So the FIR can be expressed by the following eqn (2).[25]

$$\mathrm{FIR}_1 = \frac{I_{756\ \mathrm{nm}}}{I_{540\ \mathrm{nm}}} = \frac{C_1 + C_2 \exp(-\Delta E/kT)}{C_3 + C_4 \exp(-\Delta E/kT)} \quad (2)$$

where C_1, C_2, C_3 and C_4 are constants about spontaneous emission rate, energy level degeneracy and emission energy. ΔE is the energy gap of the $^5S_2$ and $^5F_4$, k is the Boltzmann constant, and T is the absolute temperature. It can be seen in Fig. 5(d), the FIR of the $I_{756\ nm}/I_{540\ nm}$ regularly changes with the temperature increasing. It shows a nonlinear variation of FIR value at the temperature range 303 to 573 K. The eqn (2) is used to well fit the data, the C_1, C_2, C_3, C_4 and ΔE are 0.15, −0.3, 2.98, −6.1 and 429.15 cm^{-1}, respectively.

In the experiment, absolute sensitivity (S_a) is a non-negligible evaluation index of temperature, which indicates the absolute change of FIR in unit temperature, as shown in eqn (3).

$$S_a = \left|\frac{\mathrm{dFIR}}{\mathrm{d}T}\right| \quad (3)$$

Relative sensitivity (S_r) is also an important parameter that can be described as:

$$S_r = \left|\frac{1}{\mathrm{FIR}}\frac{\mathrm{dFIR}}{\mathrm{d}T}\right| \quad (4)$$

S_a and S_r of the sample are shown in Fig. 5(e) and (f), which are fitted by eqn (3) and (4). The S_a increases with the temperature enhancement, reaching a maximum of 0.0017 K^{-1} at 573 K. While the maximum value of S_r is 1.27% K^{-1} at 573 K.

Fig. 6(a) shows that the emission intensities of the green and red band vary with temperature increasing. It can see that the intensity of red emission decreases more slowly than that of green emission. The energy levels $^5S_2$,$^5F_4$ and $^5F_5$ energy levels are far apart, and the particle population at the two energy levels do not follow the Boltzmann-type distribution. The $^5S_2$, $^5F_4$ and $^5F_5$ belong to non-TCLs. So the traditional FIR analysis method based on TCLs is not appropriate for the non-TCLs system. In the previous report, the relation of the non-TCLs FIR and temperature can be fitted by eqn (5).[26]

$$\mathrm{FIR}_2 = \frac{I_{540\ \mathrm{nm}}}{I_{663\ \mathrm{nm}}} = a + bT + cT^2 \quad (5)$$

Fig. 6(b) shows that the original data for the $I_{540\ nm}/I_{663\ nm}$ as a function of the temperature fitting with the eqn (5). Consequently the FIR based on $^5S_2$, $^5F_4$/$^5F_5$ (Ho^{3+}) shows the significant temperature dependence and well fits the eqn (5). The curve of S_a and S_r by calculation and fitting are shown in Fig. 6(c) and (d). The S_a goes down with the increasing of temperature. The maximum S_a is 0.0158 K^{-1} at 303 K. While the S_r reaches a maximum of 0.41% K^{-1} at 393 K. The above analysis of the sensitivity of $SrWO_4$:Ho^{3+}/

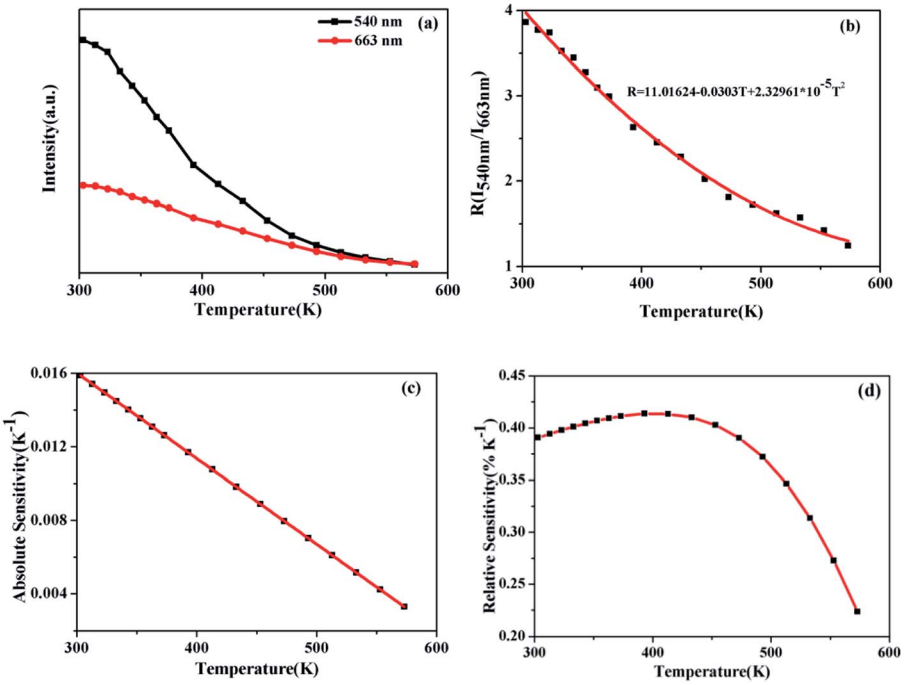

Fig. 6 (a) The emission intensity of $SrWO_4$:1%Ho^{3+}/2%Yb^{3+} phosphor center at red (663 nm) and green (540 nm) changes with temperature. (b) The FIR ($I_{540\ nm}/I_{663\ nm}$), (c) the absolute sensitivity and (d) the relative sensitivity of $SrWO_4$:Ho^{3+}/Yb^{3+} phosphor as a function of temperature.

Yb^{3+} based on the TCLs and the non-TCLs shows that the sample has high sensitivity and it has certain application value in optical temperature measurement.

Besides, the Er^{3+}–Yb^{3+} co-doped $SrWO_4$ phosphor has also been studied for its sensing properties. As shown in Fig. 7(a), the UC emission spectra of green light in the different temperature are recorded. The UC luminescence intensities of 528 nm and 550 nm (generated by $^2H_{11/2} \rightarrow {}^4I_{15/2}$ and $^4S_{3/2} \rightarrow {}^4I_{15/2}$) vary differently with the change of temperature. At 313 K, the intensity of the two emission bands is almost equal, with the

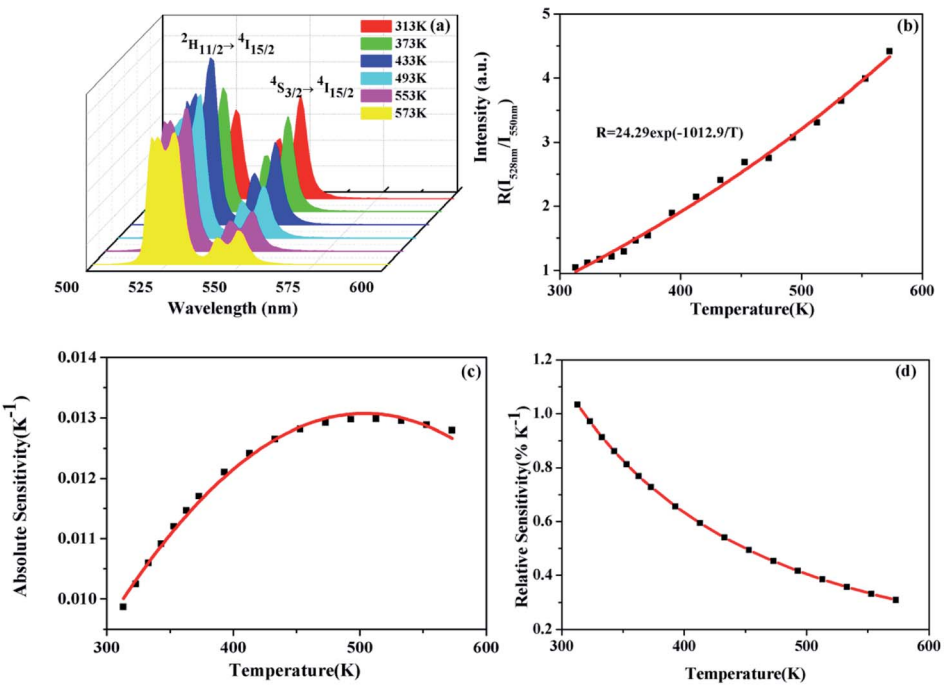

Fig. 7 (a) Temperature-dependent green UC emission spectra of 1%Er^{3+}/1%Yb^{3+} co-doped $SrWO_4$ phosphor at 313–573 K. (b) dependence of FIR for $I_{528\ nm}/I_{550\ nm}$ on absolute temperature. (c and d) The variation of absolute sensitivity and the relative sensitivity for $SrWO_4$:1%Er^{3+}/1% Yb^{3+} phosphor with temperature between 313 K and 573 K.

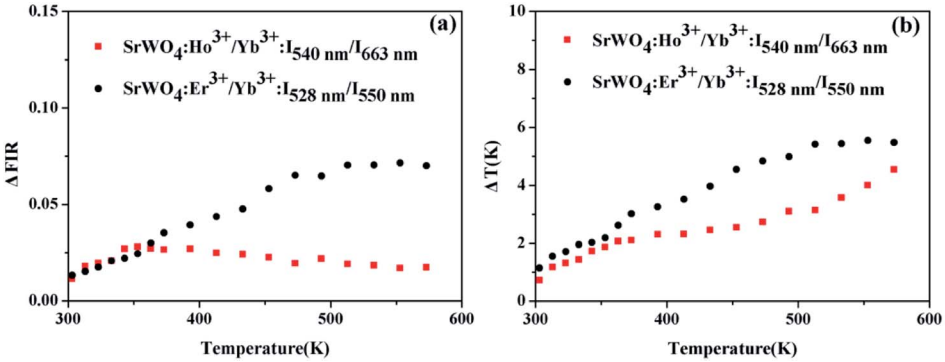

Fig. 8 (a) ΔFIR and (b) ΔT of $SrWO_4$:Ho^{3+}/Yb^{3+} based on the non-TCLs ($^5S_2$, $^5F_4$/$^5F_5$) and $SrWO_4$:Er^{3+}/Yb^{3+} based on the TCLs ($^2H_{11/2}$/$^4S_{3/2}$) pair at 303–573 K.

temperature increasing, the luminescence intensity of the 528 nm emission band is gradually increased within 313–433 K, and that of the 550 nm emission band gradually decreases. Then, in the range of 433–573 K, as the temperature increasing, the intensities of two bands also decrease because of the non-radiative relaxation enhancement. But the luminescence intensity of the 550 nm emission band decreases faster than that of 528 nm emission band. When the temperature increases, the electrons at $^4S_{3/2}$ state are excited. The transition from $^4S_{3/2}$ to $^2H_{11/2}$ occurs. It indicates that the $^2H_{11/2}$ and $^4S_{3/2}$ states of Er^{3+} can be regarded as TCLs, and the electrons population at $^2H_{11/2}$ and the $^4S_{3/2}$ states follows the Boltzmann distribution. The FIR of TCLs can be expressed by the eqn (6):[27]

$$\mathrm{FIR} = \frac{I_{528\ \mathrm{nm}}}{I_{550\ \mathrm{nm}}} = C\exp\left(-\frac{\Delta E}{kT}\right) \tag{6}$$

The changing of FIR of $I_{528\ nm}/I_{550\ nm}$ with temperature is displayed in Fig. 7(b), which is fitted by eqn (6). According to the fitting curve of the experimental data, the calculated C value is 24.29 and $\Delta E/k$ is 1012.9, so the ΔE between $^2H_{11/2}$ and $^4S_{3/2}$ is 703.7 cm^{-1}, which is very close to the experiment value of 758 cm^{-1}, the latter is obtained from the UC emission spectrum. Fig. 7(c) shows the S_a of $SrWO_4$:1%Er^{3+}/1%Yb^{3+} phosphor. The S_a of the phosphor increases at first and then decreases, reaching a maximum of 0.013 K^{-1} at 513 K. In Fig. 7(d) the S_r also is calculated, and the S_r reaches a maximum of 1.03% K^{-1} at 313 K.

In addition, thermal resolution (ΔT) is also a key parameter, which can be defined as:

$$\Delta T = \frac{\Delta\mathrm{FIR}}{\mathrm{FIR}}\frac{1}{S_r} = \frac{\Delta\mathrm{FIR}}{S_a} \tag{7}$$

where ΔFIR is the uncertainty of FIR, S_r is the relative sensitivity, and S_a is the absolute sensitivity. The ΔFIR can be calculated by the following equation.

$$\Delta\mathrm{FIR} = \frac{\sum_{i=1}^{i=n}\left|\mathrm{FIR}_i - \overline{\mathrm{FIR}}\right|}{n} \tag{8}$$

where $\overline{\mathrm{FIR}}$ and the corresponding uncertainty ΔFIR are the average and the standard deviation values from 20 measurements at each temperature, FIR_i is the i-th FIR measured at the same temperature and n is the number of measurements.

For $SrWO_4$:Ho^{3+}/Yb^{3+} phosphor, the thermal resolution of temperature measurement based on the non-TCLs ($^5S_2$, $^5F_4$/$^5F_5$) FIR has been investigated. While the thermal resolution of temperature measurement based on the TCLs ($^2H_{11/2}$/$^4S_{3/2}$) also has been discussed for $SrWO_4$:Er^{3+}/Yb^{3+} phosphor. The values

Table 1 Comparison of the maximum sensitivity of Ho^{3+}(Er^{3+})/Yb^{3+} doped in different material

Materials	Energy level	S_r (K^{-1})	S_a (K^{-1})	Reference
Bi_2SiO_5:Yb^{3+},Tm^{3+}	$^3F_{3,/2}$/$^1G_4$	1.95% (300 K)	0.0168 (300 K)	7
$NaGdF_4$:Er^{3+}/Yb^{3+}	$^2H_{11/2}$/$^4S_{3/2}$	1.29% (303 K)	0.0382 (363 K)	28
LaF_3:Er^{3+}/Yb^{3+}	$^2H_{11/2}$/$^4S_{3/2}$	844/T^{-2} (150 K)	0.0025 (400 K)	29
Y_2O_3:Ho^{3+}/Yb^{3+}/Zn^{3+}	$^5F_3$/$^3K_8$	1067.76/T^{-2} (299 K)	0.003 (673 K)	30
$NaLa(MnO_4)_2$:Sm^{3+}/Tb^{3+}	$^4G_5$/$_2$/$^5D_4$	1.93 (498 K)	0.119 (265 K)	31
$BaY_2Si_3O_{10}$:Ho^{3+}/Yb^{3+}	$^5F_5$/$^5S_2$, $^5F_4$	0.49% (298 K)	0.023 (298–448 K)	32
$BaY_2Si_3O_{10}$:Er^{3+}/Yb^{3+}	$^4F_{9/2}$/$^2H_{11/2}$	0.78% (298 K)	0.091 (298 K)	32
$LaAlO_3$:Er^{3+}/Yb^{3+}	$^2H_{11/2}$/$^4S_{3/2}$	575.27/T^{-2} (281 K)	0.0032 (281 K)	33
$NaY(WO_4)_2$:Er^{3+}/Yb^{3+}	$^2H_{11/2}$/$^4S_{3/2}$	1043.12/T^{-2} (133 K)	0.0112 (515 K)	34
$SrWO_4$:Er^{3+}/Yb^{3+}	$^2H_{11/2}$/$^4S_{3/2}$	1.03% (313 K)	0.013 (513 K)	This work
$SrWO_4$:Ho^{3+}/Yb^{3+}	$^5S_2$/$^5F_4$	1.27% (573 K)	0.0017 (573 K)	This work
$SrWO_4$:Ho^{3+}/Yb^{3+}	$^5S_2$, $^5F_4$/$^5F_5$	0.41% (393 K)	0.0158 (303 K)	This work

of ΔFIR and ΔT are presented among the range of 303–573 K in Fig. 8(a) and (b), respectively. It can be seen that the ΔFIR of $SrWO_4$:Ho^{3+}/Yb^{3+} is lower than that of $SrWO_4$:Er^{3+}/Yb^{3+}. At 303 K, the ΔT of $SrWO_4$:Ho^{3+}/Yb^{3+} and $SrWO_4$:Er^{3+}/Yb^{3+} have the minimum values of 0.72 K and 1.14 K, respectively. The values of ΔT become increasingly with the temperature enhancement. Therefore, the samples have better accuracy at lower temperature.

In order to correctly evaluate experimental results, the other materials doped with different RE ions are compared in Table 1. It can clearly conclude that the sensitivity of our sample is higher than that of the most of samples in the table.

4. Conclusion

In conclusion, the $SrWO_4$:Ho^{3+}(Er^{3+})/Yb^{3+} phosphors are successfully prepared by solid state reaction method. The UC luminescence properties of $SrWO_4$:Ho^{3+}(Er^{3+})/Yb^{3+} samples are investigated under 980 nm excitation. Furthermore, the temperature sensing properties of the Ho^{3+}:$^5S_2$/$^5F_4$ (TCLs), Er^{3+}:$^2H_{11/2}$/$^4S_{3/2}$ (TCLs) and the Ho^{3+}:$^5S_2$, $^5F_4$/$^5F_5$ (non-TCLs) are investigated in the temperature range of 303–573 K. Specifically, the absolute sensitivity value reaches 0.0158 K^{-1} at 303 K for Ho^{3+}:$^5S_2$, $^5F_4$/$^5F_5$ (non-TCLs) and the relative sensitivity value reaches 0.41% at 393 K, which is superior to most optical temperature sensing materials doped with RE^{3+} ions. It means that the $SrWO_4$:Ho^{3+}/Yb^{3+} can achieve higher absolute sensitivity by FIR of non-TCLs, as well as it has potential application in optical temperature sensors.

Conflicts of interest

There are no conflicts to declare.

Acknowledgements

This work was supported by Natural Science Foundation of China (Grant No: 61705077); Science Foundation of Jilin Province Education Department (JJKH20190853KJ); Project of Jilin Provincial Science and Technology Department (No: 20190303064SF, 20200403072SF); Project of Jilin Province Development and Reform Commission (2019C048-4, 2020C021-5).

References

1 X. F. Wang, Q. Liu, Y. Y. Bu, C. S. Liu, T. Liu and X. H. Yan, Optical temperature sensing of rare-earth ion doped phosphors, *RSC Adv.*, 2015, **5**(105), 86219–86236.

2 M. Back, E. Casagrande, E. Trave, D. Cristofori, E. Ambrosi, F. Dallo, M. Roman, J. Ueda, J. Xu, S. Tananbe, A. Benedetti and P. Riello, Confined-Melting-Assisted Synthesis of Bismuth Silicate Glass-Ceramic Nanoparticles: Formation and Optical Thermometry Investigation, *ACS Appl. Mater. Inter.*, 2020, **12**, 55195–55204.

3 S. Balabhadra, M. L. Debasu, C. D. S. Brites, R. A. S. Ferreira and L. D. Carlos, Upconverting Nanoparticles Working as Primary Thermometers in Different Media, *J. Phys. Chem. C.*, 2017, **121**(25), 13962–13968.

4 M. Back, J. Ueda, M. G. Brik and S. Tananbe, Pushing the Limit of Boltzmann Distribution in Cr^{3+}-Doped $CaHfO_3$ for Cryogenic Thermometry, *ACS Appl. Mater. Inter.*, 2020, **12**(34), 38325–38332.

5 A. Ćirić, T. Gavrilović and M. D. Dramićanin, Luminescence Intensity Ratio Thermometry With Er^{3+}: Performance Overview, *Crystals*, 2021, **11**(2), 189.

6 M. Back, E. Casagrande, C. A. Brondin, E. Ambrosi, D. Cristofori, J. Ueda, S. Tanabe, E. Trave and P. Riello, Lanthanide-Doped Bi_2SiO_5@SiO_2 Core–Shell Upconverting Nanoparticles for Stable Ratiometric Optical Thermometry, *ACS Appl. Nano Mater.*, 2020, **3**, 2594–2604.

7 E. Casagrande, M. Back, D. Cristofori, J. Ueda, S. Tanabe, S. Palazzolo, F. Rizzolio, V. Canzonieri, E. Trave and P. Riello, Upconversion-mediated Boltzmann thermometry in double-layered Bi_2SiO_5:Yb^{3+},Tm^{3+}@SiO2 hollow nanoparticles, *J. Mater. Chem. C*, 2020, **8**, 7828–7836.

8 S. S. Zhou, S. Jiang, X. T. Wei, Y. H. Chen, C. K. Duan and M. Yin, Optical thermometry based on upconversion luminescence in Yb^{3+}/Ho^{3+} co-doped $NaLuF_4$, *J. Alloys Compd.*, 2014, **588**, 654–657.

9 M. Back, J. Ueda, J. Xu, D. Murata, M. G. Brik and S. Tanabe, Ratiometric Luminescent Thermometers with a Customized Phase-Transition-Driven Fingerprint in Perovskite Oxides, *ACS Appl. Mater. Inter.*, 2019, **11**, 38937–38945.

10 S. A. Wade, S. F. Collins and G. W. Baxter, Fluorescence intensity ratio technique for optical fiber point temperature sensing, *J. Appl. Phys.*, 2003, **94**(8), 4743–4756.

11 M. Back, J. Ueda, H. Nambu, M. Fujita, A. Yamamoto, H. Yoshida, H. Tanaka, M. G. Brik and S. Tanabe, Boltzmann Thermometry in Cr^{3+}-Doped Ga_2O_3 Polymorphs: The Structure Matters, *Adv. Optical Mater.*, 2021, **9**, 2100033.

12 Y. Zhao, X. Wang, Y. Zhang, Y. Li and X. Yao, Optical temperature sensing of up-conversion luminescent materials: Fundamentals and progress, *J. Alloy Cod.*, 2020, **817**, 152691.

13 M. Back, J. Ueda, J. Xu, K. Asami, M. G. Brik and S. Tananbe, Effective Ratiometric Luminescent Thermal Sensor by Cr3+-Doped Mullite $Bi_2Al_4O_9$ with Robust and Reliable Performances, *Adv. Optical Mater.*, 2020, **8**(11), 2000124.

14 C. Shivakumara, R. Saraf, S. Behera, N. Dhananjaya and H. Nagabhushana, Scheelite-type MWO_4(M = Ca, Sr, and Ba) nanophosphors: Facile synthesis, structural characterization, photoluminescence, and photocatalytic properties, Mater, *Res Bull*, 2015, **61**, 422–432.

15 A. Y. Lan, B. Li, H. Shen and J. L. Zhang, $SrWO_4$:Ho^{3+}, Yb^{3+}, Tm3+ microspheres with white-light emission:synthesis and luminescence, *J. Mater. Sci.: Mater. Electron.*, 2015, **26**(3), 1695–1699.

16 A. Pandey, V. K. Rai, V. Kumar, V. Kumar and H. C. Swart, Upconversion based temperature sensing ability of Er^{3+}–Yb^{3+}codoped $SrWO_4$: An optical heating phosphor, *Sens. Actuators, B*, 2015, **209**, 352–358.

17 H. L. Song, C. Wang, Q. Han, X. Y. Tang, W. C. Yan, Y. F. Chen, J. F. Jiang and T. G. Liu, Highly sensitive Tm^{3+}/Yb^{3+}codoped $SrWO_4$ for optical thermometry, *Sens. Actuators, A*, 2018, **271**, 278–282.

18 H. L. Song, Q. Han, C. Wang, X. Y. Tang, W. C. Yan, Y. F. Chen, X. R. Zhao, J. F. Jiang and T. G. Liu, Optical temperature sensing properties of Sm^{3+} doped $SrWO_4$ phosphor, *Opt. Mater.*, 2018, **78**, 402–406.

19 H. L. Song, Q. Han, X. Y. Tang, X. R. Zhao, K. Ren and T. G. Liu, Nd^{3+}/Yb^{3+} codoped $SrWO_4$ for highly sensitive optical thermometry based on the near infrared emission, *Opt. Mater.*, 2018, **84**, 263–267.

20 F. Huang, Y. Gao, J. C. Zhou, J. Xu and Y. S. Wang, Yb^{3+}/Er^{3+} co-doped $CaMoO_4$: a promising green upconversion phosphor for optical temperature sensing, *J. Alloys Compd.*, 2015, **639**, 325–329.

21 J. Zhou, Y. Q. Chen, R. S. Lei, H. P. Wang, Q. G. Zhu, X. M. Wang, Y. Q. Wu, Q. H. Yang and S. Q. Xu, Excellent photoluminescence and temperature sensing properties in Ho^{3+}/Yb^{3+} codoped $(Y_{0.88}La_{0.09}Zr_{0.03})_2O_3$ transparent ceramics, *Ceram. Int.*, 2019, **45**(6), 7696–7702.

22 X. N. Chai, J. Li and X. S. Wang, Upconversion Luminescence and Temperature Sensing Properties of Ho^{3+}/Yb^{3+}-Codoped $ZnWO_4$ Phosphors Based on Fluorescence Intensity Ratios, *RSC Adv.*, 2017, **64**, 40046–40052.

23 L. Lei, D. Q. Chen, C. Li, F. Huang, J. J. Zhang and S. Q. Xu, Inverse thermal quenching effect in lanthanide-doped upconversion nanocrystals for anti-counterfeiting, *J. Mater. Chem. C*, 2018, **6**(20), 5427–5433.

24 P. Haro-González, S. F. León-Luis, S. González-Pérez and I. R. Martín, Analysis of Er^{3+} and Ho^{3+} codoped fluoroindate glasses as wide range temperature sensor, *Mater. Res. Bull.*, 2011, **46**, 1051–1054.

25 P. Du, L. H. Luo and J. S. Yu, Low-temperature thermometry based on upconversion emission of Ho/Yb-codoped $Ba_{0.77}Ca_{0.23}TiO_3$ ceramics, *J. Alloys Compd.*, 2015, **632**, 73–77.

26 H. Y. Lu, H. Y. Hao, G. Shi, Y. C. Gao, R. X. Wang, Y. L. Song, Y. X. Wang and X. R. Zhang, Optical temperature sensing in β-NaLuF4:Yb^{3+}/Er^{3+}/Tm^{3+} based on thermal, quasi-thermal and non-thermal coupling levels, *RSC Adv.*, 2016, **6**, 55307–55311.

27 X. N. Chai, J. Li, X. S. Wang, Y. X. Li and X. Yao, Color-tunable upconversion photoluminescence and highly performed optical temperature sensing in Er^{3+}/Yb^{3+} co-doped $ZnWO_4$, *Opt. Express*, 2016, **24**(20), 22438–22447.

28 J. M. Wang, H. Lin, Y. Cheng, X. S. Cui, Y. Gao, Z. L. Ji, J. Xu and Y. S. Wang, A novel high-sensitive upconversion thermometry strategy: Utilizing synergistic effect of dual-wavelength lasers excitation to manipulate electron thermal distribution, *Sens. Actuators, B*, 2019, **278**, 165–171.

29 H. J. Zhang, X. B. Dong, L. Y. Jiang, Y. Yang, X. R. Cheng and H. M. Zhao, Comparative analysis of upconversion emission of LaF_3:Er/Yb and LaOF:Er/Yb for temperature sensing, *J. Mol. Struct.*, 2020, **1206**, 127665.

30 A. Pandey and V. K. Ray, Improved Luminescence and Temperature Sensing Performance of Ho^{3+}, Yb^{3+}, Zn^{2+}: Y_2O_3 Phosphor, *Dalton Trans.*, 2013, **42**, 11005–11011.

31 Y. Zhu, Q. Meng, W. Sun and S. Lü, Sm3+, Tb3+ co-doped $NaLa(MoO_4)_2$ temperature sensing materials based on the fluorescence intensity ratio, *J. Alloys Compd.*, 2019, **784**, 456–462.

32 H. Q. Ge and J. Zhang, Investigation on luminescence properties of BaY2Si3O10:Er^{3+}/Ho^{3+}-Yb^{3+} for optical temperature sensing, *J. Mater. Sci.: Mater. Electron.*, 2018, **29**, 20033–20039.

33 G. F. Liu, L. L. Fu, Z. Y. Gao, X. X. Yang, Z. L. Fu, Z. Y. Wang and Y. M. Yang, Investigation on the Temperature Sensing Behavior in Yb^{3+} Sensitized Er^{3+} doped Y_2O_3, YAG and $LaAlO_3$ Phosphors, *RSC Adv.*, 2015, **5**(64), 51820–51827.

34 P. Du, L. H. Luo and J. S. Yu, Upconversion emission, cathodoluminescence and temperature sensing behaviors of Yb^{3+} ions sensitized $NaY(WO_4)_2$:Er^{3+} phosphors, *Ceram. Int.*, 2015, **42**(5), 5635–5641.